NLL-assisted Multilayer Graphene Patterning

Evgeniya Kovalska[1,2*], Ihor Pavlov[3], Petro Deminskyi[3], Anna Baldycheva[2],

F. Ömer Ilday[3] and Coskun Kocabas[1, 4]

[1]Laboratory of Smart Materials and Devices, Department of Physics, Bilkent University, Ankara/Turkey, 06800
[2]Department of Engineering and Centre for Graphene Science, College of Engineering, Mathematics and Physical Sciences, University of Exeter, Exeter, UK, EX4 4QF
[3]Ultrafast Optics and Lasers Laboratory, Department of Physics, Bilkent University, Ankara/Turkey, 06800
[4]Materials Science Center, School of Materials, University of Manchester, Oxford Rd., Manchester, UK, M13 9PL

E-mail: evgeniya.kovalska.ua@gmail.com

Keywords: graphene patterning; CVD-growth; non-linear laser lithography.

Abstract

The range of application of diverse graphene-based devices could be limited by insufficient surface reactivity, unsatisfied shaping, or null energy gap of graphene. Engineering the graphene structure by laser techniques can adjust transport properties and surface area of graphene, providing devices of different nature with a higher capacitance. Additionally, the created periodic potential and appearance of the active external/inner/edge surface centers determine the multifunctionality of the graphene surface and corresponding devices. Here, we report on the first implementation of nonlinear laser lithography (NLL) for multilayer graphene (MLG) structuring, which offers a low-cost, single-step, and high-speed nanofabrication process. The NLL relies on the employment of a high repetition rate femtosecond Yb fiber laser that provides generation of highly reproducible, robust, uniform and periodic nanostructures over a large surface area (1 cm^2/15 sec). NLL allows one to obtain clearly pre-designed patterned graphene structures without fabrication tolerances, caused by contacting mask contamination, polymer residuals and direct laser exposure of the graphene layers. We represent regularly-patterned multilayer graphene (p-MLG) obtained by the CVD-method on NLL-structured Ni foil. We also demonstrate tuning of chemical (wettability) and electro-optical (transmittance and sheet resistance) properties of p-MLG due to laser power adjustment. In conclusion, we show the great promise of fabricated devices, namely supercapacitors, and Li-ion batteries by using NLL-assisted graphene patterning. Our approach demonstrates a new avenue to pattern graphene for multifunctional device engineering in optics, photonics, and bioelectronics.

Introduction

The patterning and microstructuring of graphene films can selectively enhance certain (opto)electronics capabilities of graphene-based devices and can offer not only new applications, but most importantly multifunctionality of the next generation graphene-based devices for energy storage, photonics, and bioelectronics[1-4]. Engineering graphene structure restricts the motion of electrons in specific directions, for

example by forming a junction-like structure that changes from zero-gap conductor to semiconductor. Hence, when graphene is patterned into narrow ribbons[5] or ordered in accordance with substrate geometry[6] we expect the opening of an energy gap and, consequently, tuning of the transport properties of graphene-based devices. Besides, patterning increases specific surface area of graphene resulted in a higher capacity of corresponding devices. Multifunctionality of graphene surface driven by imposing a super periodic potential[7] and forming active centers (by defects, oxygen-based functional groups, self-assembly monolayers) controls graphene electronic properties consistently. Therefore, patterning of graphene could be a good approach for tuning the transport properties of graphene-based devices as well as the reactivity by increasing the surface area and artificial ordering of graphene.

Several methods which require execution of different steps for patterning procedure have been demonstrated. For example mechanical cleavage[8], scanning probe lithography[9], photocatalytic etching[10], plasma etching[11], chemical etching[11,12], assembling[13], combination soft-lithography with oxygen plasma etching[14,15] etc. Although these methods are suitable for large-scale fabrication of a variety of patterns, they involve multiple processes, and, therefore, are time-consuming and costly. Alternatively, so-called *in-situ* techniques enable to grow already patterned structure based on, for example, patterning of catalytic metal films before growth[16], laser-induced chemical vapor deposition (CVD)[17] etc. However, most of the grown materials require transfer on a desired substrate that will lead to a generation of surface and edge defects. In order to prevent disordered carbon-carbon bonds from film defects and to avoid the formation of contaminations (for example, graphene release with catalyst) the direct-writing[18,19] or cutting of already grown graphene[20,21] have been employed. Among all manufacturing techniques, only Nonlinear Laser Lithography (NLL)[22] – a new laser-based technique – is a single-step, high-speed (1 cm^2/15 sec), high-productive (does not require specified environmental conditions) and, hence, the most efficient method to fabricate small/large-scale and mask-free micro/nanopatterns of various nature and symmetry. Since 1965 the fabrication of regular nanostructures[23] on various surfaces (metals[24], semiconductors[25], and glasses[26]) was realized by laser-induced periodic surface structuring – LIPSS[27]. The main challenge is still precise quality control[26]. We propose the NLL (improved LIPSS) as a novel solution, which offers highly accurate control of the formation of nanostructures induced by ultrashort pulses. NLL initiates and regulates the metal-oxide nanostructures with unprecedented uniformity due to positive nonlocal and negative local feedback mechanisms, respectively[22]. Most importantly, a significant advantage of the method is an ability to use non-planar/3D and rough substrate surfaces that are in demand in device engineering. In this study, we report a new approach for multilayer graphene patterning with NLL technique for developing high-resolution graphene-based microstructured devices on various substrates.

We experimentally demonstrate the feasibility of predetermined patterning of multilayer graphene (p-MLG) on a nickel substrate by using a high-power femtosecond (FS) Yb fiber laser. Regularly patterned MLG is CVD grown on a surface of preliminarily structured nickel foil, followed by transfer onto the desired substrate for the characterization and device testing. The fabricated p-MLG films show high quality and morphology in comparison to the other existing fabrication methods, which is demonstrated by scanning electron microscopy (SEM), water contact angle measurement (WCA), surface free energy and adhesion calculation, Raman spectroscopy, and Fourier transform infrared spectroscopy (FTIR). We manifest electro-optical measurements on p-MLG as well as show performance of graphene-based devices in supercapacitor and battery constructions. This research provides a new approach for the first patterning of multilayer graphene with NLL technique for developing graphene-based devices.

Results and Discussion

Line nanostructure formation on MLG is performed through its growth on a pre-patterned nickel foil with precisely determined nanostructures on its surface. A schematic of the nanostructuring setup and the principle of the laser beam scanning over the substrate are illustrated in *figure 1(a)* and *figure 1(b)*, correspondingly. Detailed characterization of NLL technique is described in the *Methods Summary* part.

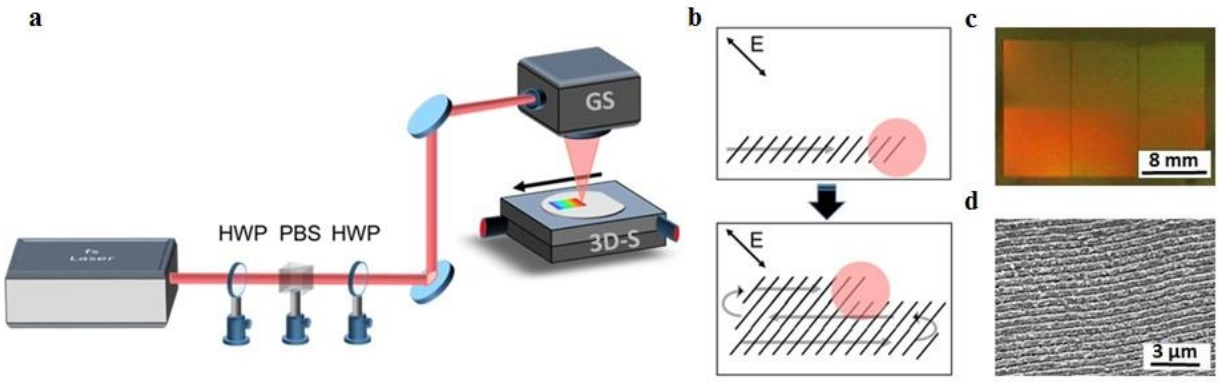

Figure 1. (**a**) Schematic image of femtosecond laser system (Yb-doped fibre laser, 1030 nm), galvanometer-scanner (GS) and motorized 3D-translation stage (3D-S); half-wave plate (HWP) and polarization beam splitter (PBS). (**b**) Scanning direction of the laser beam over the sample. The laser beam spot is represented as a pink circle. The polarization direction is indicated by an *E* vector. (**c**) Digital photo and (**d**) SEM image of structured Ni foil.

Following the nickel foil surface nanostructuring, the growth of MLG film is performed (*figure 2*). In order to achieve desirable patterns, NLL technique with coordinated adjustment of laser power (380–310 mW), scanning speed 1000 mm/s, and 10 µm spot size is provided. We used 50 µm thick structured nickel foil as a catalyst for MLG synthesis in the chemical vapor deposition system. The growth is carried out in the mixture of argon (Ar) and hydrogen (H_2) atmosphere. The methane (CH_4) is a source of carbon which arises from the gas decomposition under high temperature. Graphene patterns on the nickel foil are transferred onto the polyvinyl chloride (PVC, Sigma, Lamination foils) using lamination technique[28], afterward, nickel is etched in 1M iron (III) chloride hexahydrate solution (98%, Sigma-Aldrich item #207926).

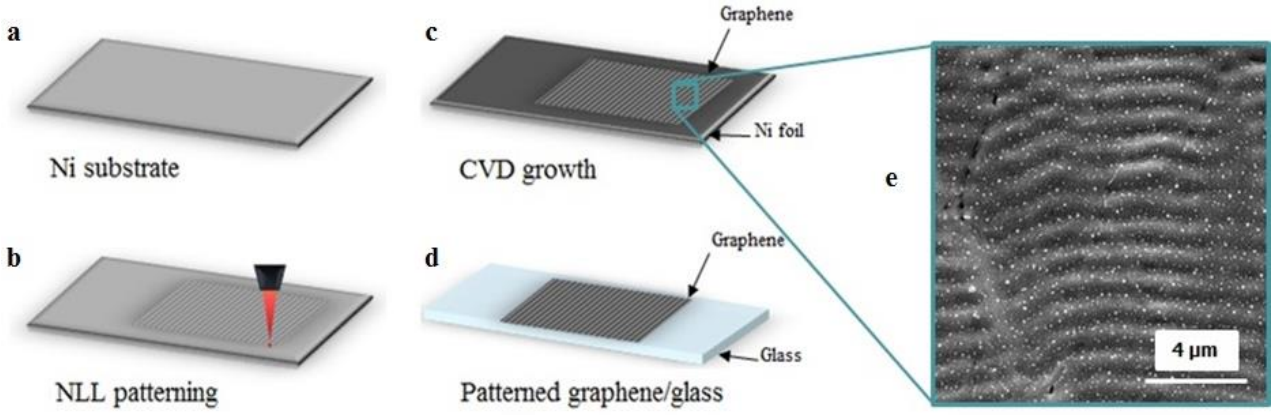

Figure 2. Schematic image of «step-by-step» patterning of graphene. (**a**) Nickel foil which (**b**) preliminary-structured with NLL technique applying various laser power (380–310 mW). (**c**) CVD-grown patterned MLG on the structured nickel foil. (**d**) Patterning of MLG transferred onto the glass. (**e**) SEM image of the p-MLG.

Figure 3 demonstrates the morphology and surface characteristics of obtained graphene patterns on the PVC substrate. The depth of the grooves on the MLG surface produced via laser structuring of the Ni catalyst is gradually reduced by decreasing the laser power for every 10 mW (*figure 3(a)*). We observe disordering of graphene surface and formation of a larger number of grain boundaries and defects. It turns out that the alignment of graphene nanostructures directly depends on the deepness of patterns in Ni foil, and the resultant graphene pattern serves as a holding lattice.

Tailoring of graphene surface wettability and understanding its response to different environmental conditions are the major steps toward development of efficient graphene-based appliances in biosensorics[29].

To characterize the surface capabilities of graphene patterns we place a drop of deionized water (DI) on the surface of pristine and patterned MLG (*figure 3(b)*). Obviously, the location of water drops indicates distinctive wettability of graphene's zones at less/equal 90 degrees of contact angle (*figure 3(c)*). Normally single-layer graphene is hydrophilic that means its water contact angle (WCA) is ≤ 90° (corresponds to a high wettability) and graphene surface is chemically active[30]. When we increase the number of graphene

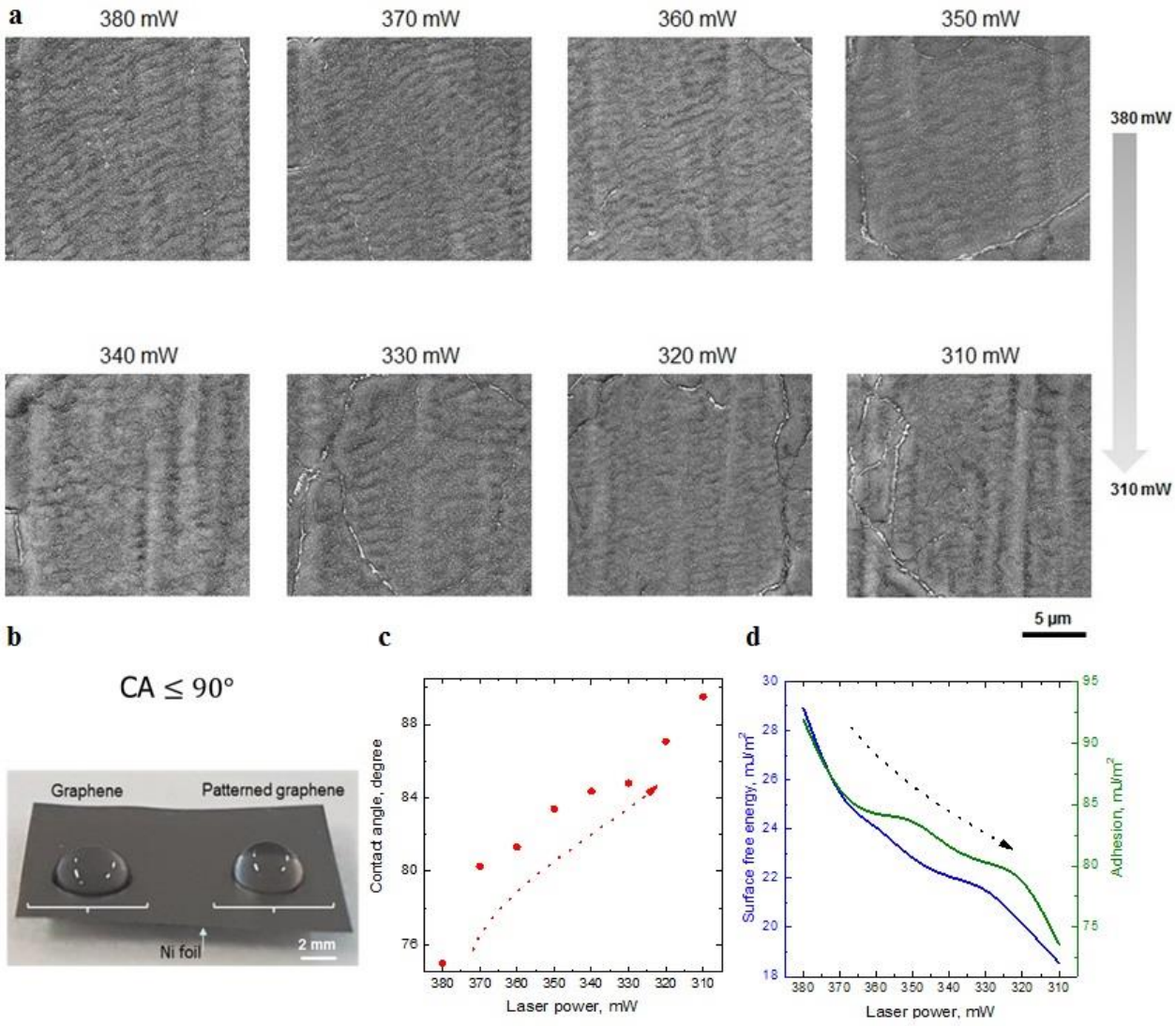

Figure 3. (**a**) Morphology and surface characteristics of patterned multilayer graphene. SEM images of CVD- synthesized p-MLG on structured Ni foil by an FS laser power treatment from 380–310 mW. The 5µm scaled images obtained at 30V, 11000–14000× magnification. (**b**) Digit photograph of placing a drop of deionized water on the surface of pristine and patterned MLG. (**c**) Water contact angle (θ) on patterned MLG surface, (**d**) adhesion (W_{pw}), and surface free energy (γ_p) versus laser power structuring; an error is ±5 units.

layers, the WCA is about ≥ 90° that corresponds to a low wettability[31]. It implies that the surface of MLG is hydrophobic and consequently more inert. But in this study, we demonstrate an opposite result – the surface of MLG is hydrophilic. *Figure 3(c)* shows a variation of the contact angle as a function of laser power. It is observed that WCA increases from a value of 75° to 89.52° after gradual laser treatment of MLG surface and this value remains nearly 90° (*figure S1, table ST1*). Although WCA data provide valuable information on the wettability of the p-MLG surface, another surface features – adhesion (W_{pw}) and surface free energy (γ_p) are the key parameters characterizing the surface and its interaction with other materials. Besides these parameters are closely related not only to wettability but also many other important properties at the surface/interface and friction[32]. Therefore, we calculated the adhesion and surface free energy of graphene patterns based on the contact angle data by the Young-Dupre equations[33]: $\gamma_w(1 + \cos\theta_0) = W_{pw}$ and $\gamma_p = \gamma_w/4(1 + \cos\theta_0)^2$, where θ_0 is the contact angle at equilibrium, γ_w is the water surface energy (73 mJ/m^2), W_{pw} is the adhesion energy of the water to MLG surface, and γ_p is the surface free energy.

Hence we determined that surface energy of the p-MLG is mutually opposite to the water contact angle values and by estimating data from *Tab. 1S* we found the highest and lowest surface energies of the p-MLG samples – 28.92 mJ/m^2 (WCA = 75°) and 18.56 mJ/m^2 (89.52°), respectively. Moreover, the surface energy caused by adhesion forces which are the reason of formation of the surface bonds. Values of surface energy and adhesion are always linearly proportional (*figure 3(d), figure S2, S3*), thus higher surface energy corresponds to a higher adhesion and vice versa. Our results indicate lower surface free energy of all patterned graphene samples than the surface free energy of water that means water partially wets out graphene surface. The graphene roughness formed by laser power treatment from 380 to 310 mW determines the increasing of the water contact angle and the surface free energy reduction, in other words, a degradation of the wettability and adhesion. The surface of graphene produced with 310 mW laser power in comparison with the rest of samples is more hydrophobic.

To characterize the graphene patterns grown on variously structured Ni foils, Raman spectroscopic analysis is performed using the laser excitation of 532 nm (*figure 4(a)*). For single Raman measurements, 20× objective and 20 s integration time are used. Collected Raman spectra are typical profiles of a few/multilayer graphene. The main G- and 2D-peaks of graphene are clearly observed at around 1578 cm^{-1} (similar for all samples) and 2695–2706 cm^{-1}, respectively. Fixed position of G-peaks (*figure 4(b)*) indicates stability in the planar vibrational mode of sp^2–hybridized carbon arrangement and consequently determines resemblance of graphene nature for all obtained patterns. The negligible 2D-band shape differences and its blue shift with decreasing of laser power during surface structuring caused by decreasing of thickness/number of graphene layers[34] (*figure 4(b)*). Analyses of the peak intensity ratio of the 2D- and G-bands is performed (*table ST2, figure S4*). The $I_{2D/G}$ ratio of these bands for all-graphene patterns is equal or less than «1» that indicates

few/multilayeredness. The appearance of low-intensity D-band in each case corresponds to the defect formation. Defectiveness stimulated by laser beam via its contact with Ni surface is manifested as a fingerprint of the already imperfect structure. Nevertheless, the relatively stable $I_{2D/G}$ ratio in terms of laser power and sharp symmetric 2D-bands are the confirmation for a high quality patterned few/multilayer graphene.

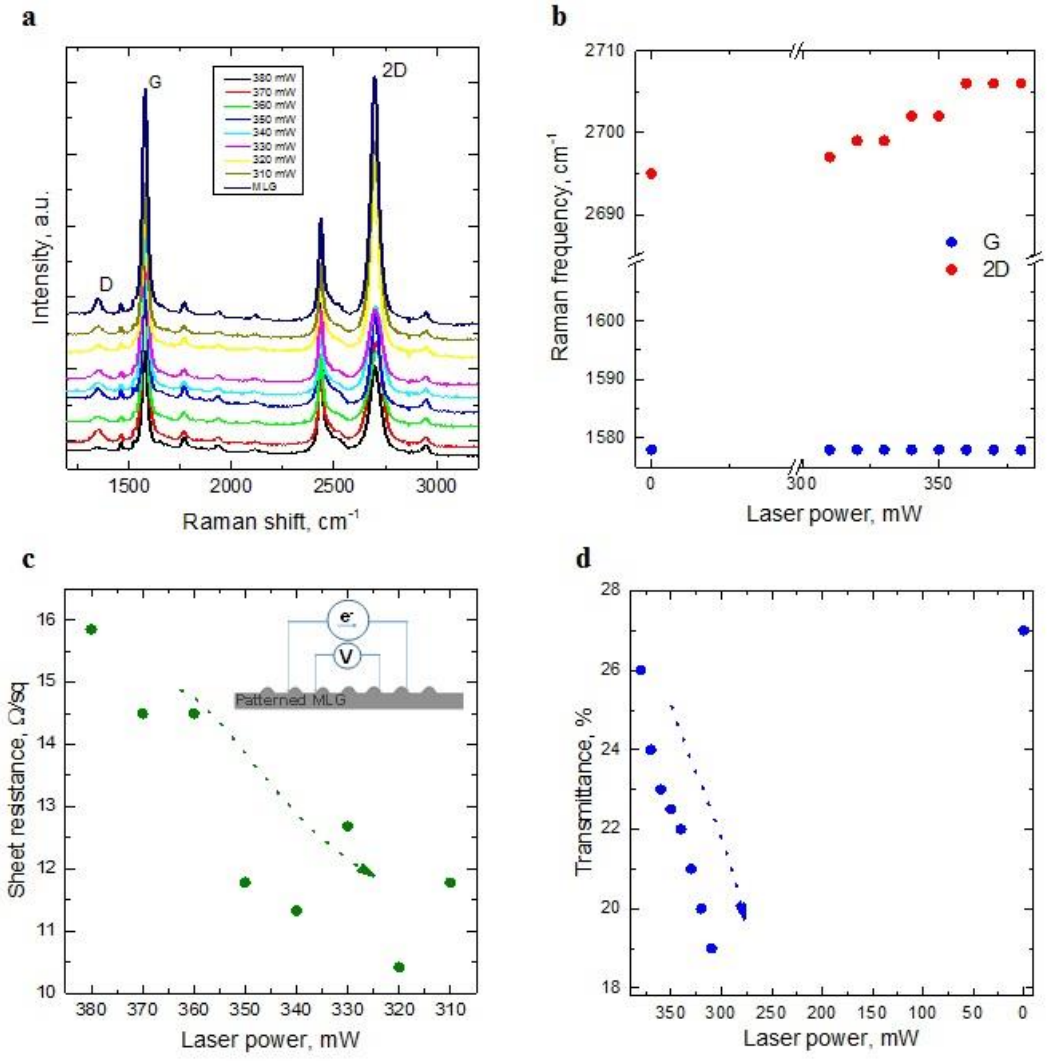

Figure 4. Optical and electrical properties of the patterned multilayer graphene. (**a**) General view of Raman spectra (G-, D-, and 2D-peaks) of MLG with different patterns. (**b**) Variation of Raman frequency as a function of laser power. (**c**) Variation of the sheet resistance of p-MLG as a function of laser power. The insertion shows the schematic representation of the four-point measurement system. (**d**) Optical transmittance of the p-MLG on the PVC substrate v.s. laser power.

Since the groove's depth of the p-MLG gradually decreases and the graphene surface roughness increases and becomes hydrophobic under laser treatment, the electrical transport property of the graphene can be tuned by the surface morphology of the created patterns. Thus, the sheet resistance (*figure 4(c)*) and optical transmittance (*figure 4(d)*) of p-MLG transferred on PVC substrate are measured and demonstrated that patterning reduces sheet resistance from 16 to 10 Ω/sq, despite the fact that obtained p-MLG already possess low sheet resistance (about 20 Ω/sq). Besides, we identified a directly proportional correlation between laser power and the sheet resistance of grown graphene patterns: each reduction in laser power of pattern processing reduces the sheet resistance of obtained p-MLG (e.g. 380 mW corresponds to 16 Ω/sq and 310 mW corresponds to 10 Ω/sq).

A variation of optical transmittance of the p-MLG on the PVC substrate at around 800 nm as a function of laser power is shown in *figure 4(d)* and *figure S5, S6*. We observed in about 1.5 times enhancement of optical transmittance with increase of laser power from 310 to 380 mW. It is known, when a number of layers increases, the thickness becomes more uniform and results in decreasing of optical transmittance[35]. Apparently sheet thickness of wrinkle configurations changes – decreasing[32] with applied lower laser power. It means that thinner and severe wrinkle-like ordering of graphene with deeper structuring (380 mW-obtained p-MLG) provides enhanced optical transmittance.

Based on the detailed morphological and electro-optical investigation of p-MLG samples, structures fabricated under 380 mW are selected. Such a graphene pattern possesses distinct structure alignment acting as a holding lattice which prevents defects appearance. It provides low sheet resistance (16 Ω/sq) and higher optical transmittance in comparison with other graphene patterns. Additionally, the thickest 380 mW-obtained p-MLG is more hydrophilic regarding another proposed variety of patterns. The hydrophilicity provides reactivity of graphene patterns and impacts its surface area which will significantly affect the performance of graphene-based devices. Therefore, we employed 380 mW-obtained p-MLG for supercapacitor and Li-ion battery designs and compared its performance with respect to the flat graphene-based devices.

We demonstrate the optical features of graphene-enabled supercapacitor behaving as an optical modulator. *Figure 5(a)* shows the schematic image of a supercapacitor preparation. The process begins from a hot lamination of MLG/p-MLG with PVC followed by etching of nickel in 1M $FeCl_3 \times H_2O$ solution. After the transfer printing process, we attached two graphene coated PVC substrates using 250 μm thick adhesive frames and affixed two copper wires in order to apply a voltage to the graphene electrodes covered with silver-based conductive ink. Created supercapacitor's cell was filled with 50 μL of ionic liquid electrolyte [DEME][TFSI] (98.5%, diethyl methyl (2-methoxyethyl)ammonium bis(trifluoromethyl sulfonyl)imide, Sigma-Aldrich item # 727679).

The change of the optical transmittance of a supercapacitor with patterned (*figure 5(b)*) and flat MLG electrodes (*figure 5(c)*) is measured by using a Bruker Vertex 70V FTIR spectrometer in which the spectral range is from 500 to 1100 nm. The optical change is performed by applying a voltage in the range of 0 to 5V for both devices; the transmission condition is normalized at 0V that confirms a stability of supercapacitors. At 0V, the transmittance is only 1-2% for both devices and slightly varies with the wavelength. Applying 5V for MLG-enabled device, the transmittance increases sharply to 19% at 750 nm, while applying 3.5V for p-MLG-enabled device, the transmittance increases at first to 16% at 950 nm. At 5V supercapacitor based on p-MLG demonstrates the second stage of the transmittance increase – 32% at 800 nm.

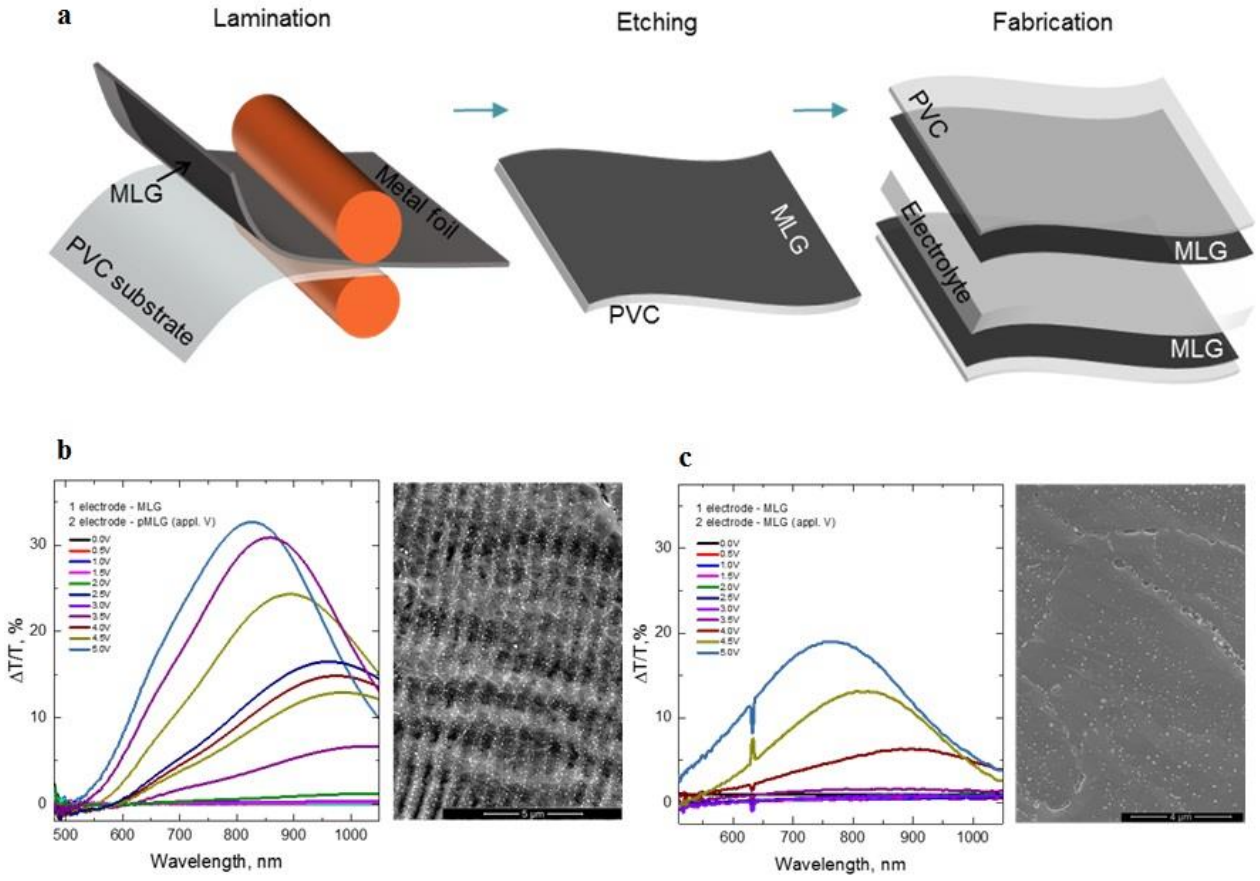

Figure 5. MLG-enabled supercapacitor. (**a**) Schematic image of a supercapacitor preparation: 1st stage – lamination with a PVC at 120°C, 2d stage – etching of catalyst with 1M iron chloride solution and 3d stage – device fabrication. Normalized change in the transmission of a supercapacitor with (**b**) patterned and (**c**) flat multilayer graphene electrodes using an ionic liquid as an electrolyte for bias voltage in the range of 0 to 5V.

Observed «2» times transmittance value increase of the device with p-MLG regarding the MLG-based device indicates the double stepwise electrostatic doping effect on graphene happened during intercalation of electrolyte: at first in the thinner part (grooves) and then in the thicker part (wrinkles). As a result, the transmittance enhancement occurs due to the light beam interaction with patterns where the p-MLG thickness is reduced – grooves part. At this point, the light scattering decreases and light transmission increases accordingly. Therefore, the light throughput of the p-MLG-enabled device will be higher with respect to MLG-enabled device.

We also defined high modulation depth[36] of about 9 dB and 6 dB for p-MLG- and MLG-based devices respectively. Since the variety of optical modulators applications is determined by high modulation depth (>7 dB, as high-rate interconnects and high-sensitivity sensing) and limited when modulation depth is less than <~4 dB (as passive mode-locking and short-distance data transmission)[37], it is crucial to acquire the modulation depth increasing. Our results indicate broader applicability for p-MLG-enabled devices and its capability to operate in the visible range as far as we are able to increase modulation depth index in 1.5 times.

Figure 6 represents graphene-enabled battery structured as a typical Li-ion battery. This device posturizes a one cell battery, where electrodes sandwiched symmetrically (*figure 6(a), 6(b)*). As an anode, we placed MLG/p-MLG on the polymer substrate, which acted as an electrochromic layer as well. In order to make good contact, we set copper frame attached to graphene-electrode. A lithium nickel manganese cobalt oxide (known in a battery manufacturing as an NMC, LITARION) operated as a charge counter electrode – cathode, providing a reversible electrochemical reaction. Finally, the electrodes are separated using 20 μm thick porous polyethylene membrane (PE, 42% porosity, Targray) soaked with 1 M lithium hexafluorophosphate solution in ethylene carbonate and ethyl methyl carbonate (Sigma-Aldrich item # 746738).

We measured the capacitance of MLG-enabled Li-ion battery at approximately 250 times demonstrating negligible decreasing of its value with each next charging/discharging cycle (*figure 6(c)*). Inherently all batteries gradually discharge eventually whether they are used or not. This capacity loss is typically caused by slow parasitic reactions occurring within the battery. The life-cycle is the key for a good performance of a battery, and thus increasing the life-cycle is one of the first parameters that should be focused on when aiming at providing efficiency of Li-ion batteries. Usually, heteroatom doping, chemical impregnating and hybridization of graphene electrodes are the best approaches to improve prolongation of Li-ion batteries. For example, graphene hybrid based battery can yield 400 discharge/charge cycles with 0.01% capacity-loss per cycle[38]; battery, where graphene electrode is impregnating with sulfur, demonstrates ultra-long viability (2000 cycles and 0.028% capacity-decay per cycle)[39]. In our case, the proposed battery with pure

MLG demonstrated operation for 1000 cycles (*figure 6(d)*), that together with assessed capacity (0.01% capacity loss per cycle) already demonstrate promising result.

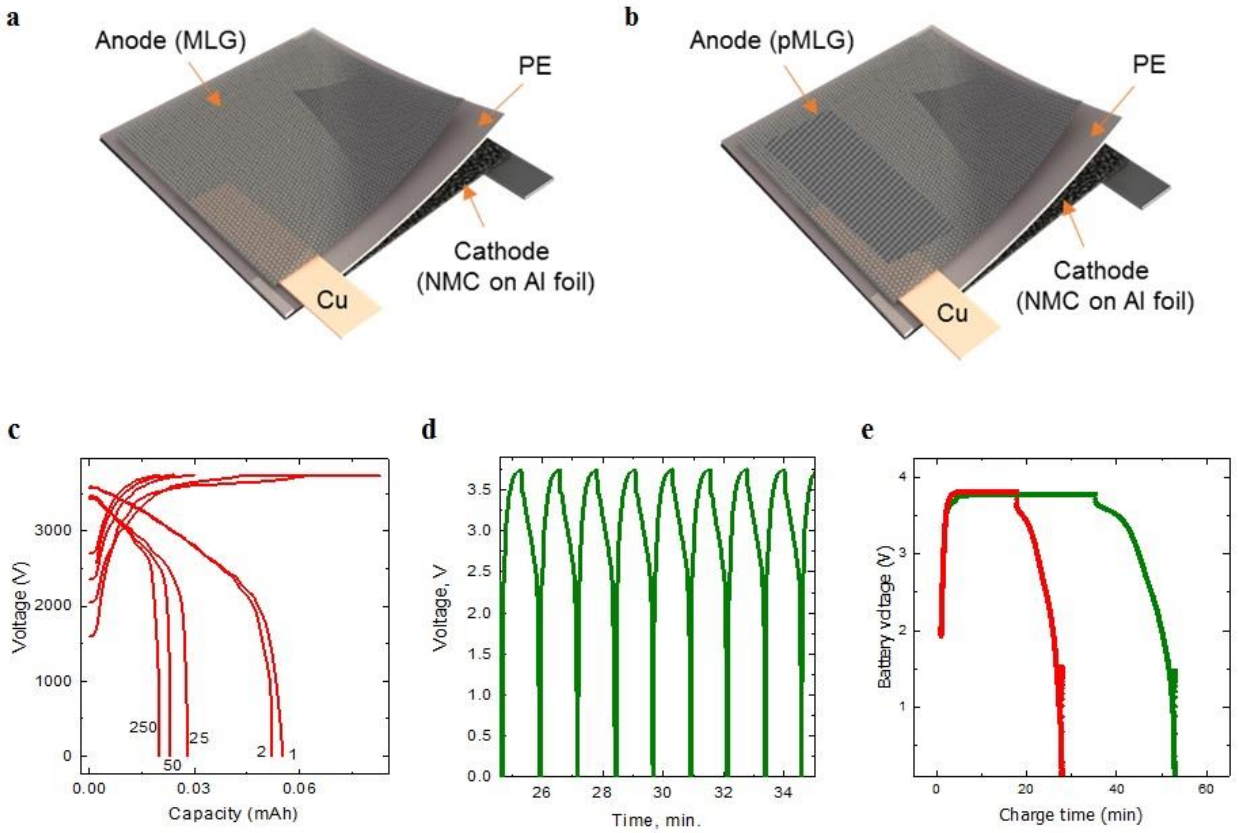

Figure 6. Graphene-enabled Li-ion battery. (**a**) Schematic image of the symmetrically constructed secondary battery based on the flat and (**b**) patterned MLG. MLG/p-MLG acted as an electrochromic layer (anode). Lithium nickel manganese cobalt oxide operated as a charge counter electrode (cathode), providing a reversible electrochemical reaction in devices operating in the transmissive/reflective modes. (**c**) Galvanostatic discharge/charge curves of MLG-based battery after 1st, 2nd, 25th, 50th, 250th measurements and (**d**) its life-cycle as a function of time. (**e**) Voltage profiles for the constant current charge and discharge of Li-ion batteries incorporating MLG (green curve) and p-MLG (red curve) as a negative electrode. The optical change results from electric current of ≈ 3 mA at low dc potentials.

On the other hand, the internal charge/discharge efficiency plays a key role as well, since slow discharging and fast charging designed in a way to reduce the impact of self-heating is required. In order to analyze batteries performance, the voltage dependence of charging/discharging processes applying constant current (3 mA) for both devices are provided (*figure 6(e)*). We observed productivity reducing of p-MLG-based battery in relation to MLG-based battery due to a decreasing of charge/discharge time by approximately «2»

times. This allows us to predetermine viability of p-MLG-enabled Li-ion battery during 500 cycles. The reduction in the number of life-cycle is due to the change in the graphene surface area after patterning procedure. In fact, the patterns are artificially ordered defects that make graphene structure more loosened and promote faster intercalation/deintercalation of Li-ions. Therefore, presented approach could lead to new bi-functional applications combining properties of energy storage and electrically switchable devices.

Conclusions

In conclusion, we demonstrate a novel NLL technique for the patterning of MLG via Ni catalyst substrate pre-structuring. NLL provides contamination-free pattern replications into varying geometrical shapes and sizes with a possibility to transfer p-MLG on the diverse substrates. The regulation of hydrophobic/hydrophilic properties of graphene by various laser power aligning are shown. Controlling of hydrophobic/hydrophilic properties defines multifunctionality of graphene-enabled devices due to the graphene surface (dis)ordering, and consequently, a formation of reactive oxygen-based functional groups. Distinct graphene structure alignment (which prevents defects appearance) assisting by strongest laser power (380 mW) contributes to certain p-MLG electro-optical changes (sheet resistance decreasing and optical transmittance enhancement). The p-MLG ability to operate as an electrically reconfigurable medium for supercapacitor and Li-ion battery designs are represented. The p-MLG-based supercapacitor testing results reveal two times transmittance value increase (in comparison with MLG-based supercapacitor) caused by light interaction with patterned structures where its thickness is reduced. The p-MLG-based battery indicates long-life viability (500 charging/discharging cycles) with 0.01% capacity-loss per cycle; negative feedback leading toward twice device productivity reducing occurred due to the graphene structure loosening after patterning and, consequently, (de)intercalation processes accelerating. We anticipate the NLL-based p-MLG to be a new approach to overcome limitations imposed by existing post-synthesis processes which will open wide applicability gateway for advanced graphene-based devices in energy storage, wearable electronics, and biosensorics.

Methods Summary

Nonlinear laser lithography

The nanostructuring setup consists of femtosecond laser system, galvanometer-scanner, and motorized 3D-translation stage (*Figure 1*). The femtosecond system is home-made Yb-doped fiber laser (1030 nm) which was reported before[40]. It involves dispersion managed type oscillator, fiber stretcher, several amplification stages and grating compressor. The stretcher fiber was distributed between amplifier stages to provide the optimal pulse peak power during amplification in order to balance between gain narrowing and self-phase modulation. The laser can produce up to 1 μJ of pulse energy at a repetition rate of 1 MHz which corresponds

to 1 W of average power. The minimal pulse duration which can be obtained from the system is 100 fs. Since the output light of the laser is linearly polarized, the half-wave plate placed between the laser and polarization beam splitter provides control of the laser power on the sample. The second half-wave plate allows control of polarization on a sample. The sample was placed on motorized 3D-stage in the focal plane of galvanometer-scanner's f-theta lens.

The laser beam was scanned over the nickel surface in the way, that during every line scan it was partially overlapped with already created structure. In this way we preserved the concept of Nonlinear Laser Lithography[22], which allows coherent extension of the created structure over a large area surface, thus, improving the quality of the structure. The maximum scanning area for our model of galvanometer-scanner is 1×1 cm^2. In order to extend the area, XY translation stage was used. With given pulse energy and repetition rate, the processing speed in our work was as fast as 15 s for 1×1 cm^2 area. It can be increased in the future by scaling repetition rate of the laser by keeping pulse energy constant i. e., simultaneously scaling average power.

CVD growth of multilayer graphene

Chemical vapor deposition system was used for growing of multilayer graphene. The growth process was carried out under ambient pressure in a 3" quartz tube furnace, using 50 μm thick Ni foil. Argon gas was flushed into quartz tube for at least 5 min in order to remove oxygen. Afterward, hydrogen was supplied while argon continued to run (ratio of Ar/H_2 is about 100/100 sccm). Gas-filled CVD system was left for heating till temperature is raised to 1000°C. Once 1000°C temperature was reached a methane flow is established at 30 sccm together with the Ar/H_2 flow at 100/100 sccm, followed by a waiting time of 5min. In the end, the CH_4 flow is turned off and the system is cooled down to room temperature in ~ 1 hrs while keeping the Ar/H_2 flow environment at 100/100 sccm.

Transfer-printing of multilayer graphene

The following steps are needed for the analysis of MLG/p-MLG surface and fabrication of graphene-enabled devices after the CVD growth on Ni foil. Firstly, one side of the graphene-covered Ni foil was protected by paper while other side was touched with PVC. Secondly, the patch of paper/graphene/Ni/graphene/PVC was sent through lamination machine with a temperature of about 120°C. The obtained PVC/graphene/Ni samples were then dipped in a 1M $FeCl_2$ aqueous etching solution for a few hrs. After the nickel was etched, the PVC/graphene membranes were placed in deionized water for a few hrs of rinsing as well. Then the samples were blow dried with N_2 gas and were ready to use.

Characterization methods

Water contact angle of MLG/p-MLG on PVC substrate was obtained using home build contact angle measurement setup. The setup consists of the following elements: white LED, XYZ translation stage with standard micrometers (Thorlabs), video camera (Thorlabs, DCC1645C – USB 2.0 CMOS Camera, 1280 x 1024, Color Sensor) and usual medical syringe with 200 um diameter needle. We put DI water droplet of 4 μL on the investigated graphene surface and took digital photos. We measured contact angles using program Screen Protractor which allows us to easily and quickly measure any angle on the screen to the nearest degree. The morphological analyses of investigated graphene samples were performed using Scanning Electron Microscopy (NOVA NANOSEM 600). To determine a graphitization fingerprint and compare defectiveness of MLG and p-MLG surfaces Jobin Yvon Horiba Raman Microscope System with 20× microscope objectives and 20 s integration time were used. The excitation wavelength was 532 nm. The transmittance measurements in the wavelength range between 450–1100 nm were performed by using Bruker Vertex 70 V Fourier Transform Infrared Spectrometer integrated with Si photodiode. The sheet

resistance measurements were carried out at Four Probe Station Platforms with a support of Keithley-2600 multimeter. MLG was attached on the patterned area to make ohmic contact with four electrodes. Then, sheet resistance was calculated using the standard formula ($Rs = \pi R/\ln 2 \approx 4.53R$).

Device's performance characterization

Graphene-Enabled Supercapacitors: Optical measurements were performed in the 450–1100 nm wavelength range by Bruker Vertex 70 V Fourier Transform Infrared Spectrometer equipped with Si photodiode. Transmittance, $T_p(\lambda)$, spectra were recorded while graphene-based supercapacitors biased using Keithley 2400 Source measure unit.

Graphene-Enabled Li-ion Battery: The voltage and time readings of charging/discharging processes were generated using the Keithley 2600 Source Meter instrument. The data were collected under a constant current at 3 mA and processed with a LabView software.

Supplementary Information

Surface characteristics of patterned MLG: water contact angle measurement, surface free energy and adhesion estimations (*Fig. S1, S2 and S3, Tab. ST1*). Raman characterization (*Tab. ST2, Fig, S4*). Optical characterization (*Fig. S5 and S6*).

Notes

The authors declare no competing financial interest.

Acknowledgement

This research was partially supported by the European Research Council (ERC) Consolidator Grants ERC-682723 SmartGraphene and ERC-617521 NLL; the European Union funding: Marie Curie Fellowship visiting grant; and the Engineering and Physical Sciences Research Council (EPSRC) of the United Kingdom via Grant No. EP/N035569/1. We thank our colleagues Dr. Nurbek Kakenov, Dr. Osman Balci and Dr. Nassima Afshar Imani from Bilkent University who provided insight and expertise that greatly assisted the research. We thank Dr. Omer Salihoglu (TUBITAK, Marmara Research Center) for assistance with capacity and life-cycle battery measurements, and Mr. Murat Güre and Mr. Ergun Karaman (physicists and engineers of Bilkent University) for catalyst preparation and technical support. Evgeniya Kovalska would also like to show her gratitude to all co-authors for sharing their pearls of wisdom and comments during the preparation of manuscript that greatly improved its quality.

Author information

Evgeniya Kovalska: evgeniya.kovalska.ua@gmail.com

Ihor Pvalov: pavlov.iop@gmail.com

Petro Deminskyi: p.deminskyi@gmail.com

Anna Baldycheva: a.baldycheva@exeter.ac.uk

F. Omer Ilday: ilday@bilkent.edu.tr

Coskun Kocabas: coskunkocabas@gmail.com

References

[1] Castro N. *et al.* 2009 The electronic properties of graphene. *Reviews of Modern Physics* **81**, 109.

[2] Choi W. *et al.* 2010 Synthesis of graphene and its applications: A review. *Critical Reviews in Solid State and Materials Sciences* **35**, 52.

[3] Shao Y. *et al.* 2010 Graphene based electrochemical sensors and biosensors: A review. *Electroanalysis* **22**, 1027.

[4] Zhang Y. *et al.* 2013 Review of chemical vapor deposition of graphene and related applications. *Accounts of Chemical Research* **46**, 2329.

[5] Han M.Y. *et al.* 2007 Energy band-gap engineering of graphene nanoribbons. *Physical Review Letters* **98**, 206805.

[6] Hicks J. *et al.* 2013 A wide-bandgap metal–semiconductor–metal nanostructure made entirely from graphene. *Nature Physics* **9**, 49.

[7] Järvinen P. *et al.* 2013 Molecular self-assembly on graphene on SiO_2 and h-BN substrates. *Nano Letters* **13**, 3199.

[8] Kang S.J. *et al.* 2011 Inking elastomeric stamps with micro-patterned, single layer graphene to create high-performance OFETs. *Advanced Materials* **23**, 3531.

[9] Tapaszto L. *et al.* 2008 Tailoring the atomic structure of graphene nanoribbons by scanning tunneling microscope lithography. *Nature Nanotechnology* **3**, 397.

[10] Zhang L. *et al.* 2011 Photocatalytic patterning and modification of graphene. *Journal of the American Chemical Society* **133**, 2706.

[11] Jiao L. *et al.* 2009 Narrow graphene nanoribbons from carbon nanotubes. *Nature* **458**, 877.

[12] Kosynkin D.V. *et al.* 2009 Longitudinal unzipping of carbon nanotubes to form graphene nanoribbons. *Nature* **458**, 872.

[13] Wei Z. *et al.* 2013 Direct writing on graphene «paper» by manipulating electrons as «invisible ink». *Nanotechnology* **24**, 275301.

[14] Feng J. *et al.* 2012 Patterning of graphene. *Nanoscale* **4**, 4883.

[15] Pang S. *et al.* 2009 Patterned graphene electrodes from solution-processed graphite oxide films for organic field-effect transistors. *Advanced Materials* **21**, 3488.

[16] Kim K.S. *et al.* 2009 Large-scale pattern growth of graphene films for stretchable transparent electrodes. *Nature* **457**, 706.

[17] Park J.B. *et al.* 2011 Fast growth of graphene patterns by laser direct writing. *Applied Physics Letters* **98**, 123109.

[18] El-Kady M.F. *et al.* 2012 Laser scribing of high-performance and flexible graphene-based electrochemical capacitors. *Science* **335**, 1326.

[19] Strong V. *et al.* 2012 Patterning and electronic tuning of laser scribed graphene for flexible all-carbon devices. *ACS Nano* **6**, 1395.

[20] Chang T.L. *et al.* 2016 Patterning of multilayer graphene on glass substrate by using ultraviolet picosecond laser pulses. *Microelectronic Engineering* **158**, 1.

[21] Kalita G. *et al.* 2011 Femtosecond laser induced micropatterning of graphene film. *Materials Letters* **65**, 1569.

[22] Oktem B. *et al.* 2013 Nonlinear laser lithography for indefinitely large-area nanostructuring with femtosecond pulses. *Nature Photonics* **7**, 897.

[23] Sipe J.E. *et al.* 1983 Laser-induced periodic surface structure I: theory. *Physical Review B* **27**, 1141.

[24] Ardron M. *et al.* 2014 A practical technique for the generation of highly uniform LIPSS. *Applied Surface Science* **313**, 123.

[25] Bonse J. *et al.* 2012 Femtosecond laser-induced periodic surface structures. *Journal of Laser Applications* **24**, 042006.

[26] Sun Q. *et al.* 2008 Nanograting formation on the surface of silica glass by scanning focused femtosecond laser pulses. *Optical Letters* **33**, 2713.
[27] Birnbaum M. 1965 Semiconductor surface damage produced by ruby lasers. *Jouran of Applide Physics* **36**, 3688.
[28] Martins L.G.P. *et al.* 2013 Direct transfer of graphene onto flexible substrates. *Proceedings of the National Academy of Sciences* **110**, 17762.
[29] Xu K. *et al.* 2013 Wetting: Contact with what? *Nature Materials* **12**, 872.
[30] Li Z. *et al*. 2013 Effect of airborne contaminants on the wettability of supported graphene and graphite. *Nature Materials* **12**, 925.
[31] Raj R. *et al.* 2013 Wettability of Graphene. *Nano Letters* **13**, 1509.
[32] Chaudhury M.K. *et al.* 1996 Interfacial interaction between low-energy surfaces. *Materials Science and Engineering: R: Reports* **16**, 97.
[33] Duca M.D. *et al*. 1998 Surface modifications of polyvinylidene fluoride (PVDF) under rf Ar plasma. *Polymer Degradation and Stability* **61**, 65.
[34] Ferrari A. C. *et al.* 2006 Raman spectrum of graphene and graphene layers. *Physical Review Letters* **97**, 187401.
[35] Shou-En Zhu *et al.* 2014 Optical transmittance of multilayer graphene. *Europhysics Letters* **108**, 17007.
[36] Reed G.T. *et al.* 2010 Silicon optical modulators. *Nature Photonics* **4**, 518.
[37] Sun Z. *et al.* 2016 Optical modulators with 2D layered materials. *Nature Photonics* **10**, 227.
[38] Sun Y. *et al.* 2013 Reconstruction of conformal nanoscale MnO on graphene as a high-capacity and long-life anode material for lithium ion batteries. *Advanced Functional Materials* **23**, 2436.
[39] Zhou G. *et al.* 2014 A graphene-pure-sulfur sandwich structure for ultrafast, long-life lithium–sulfur batteries. *Advanced Materials* **26**, 625.
[40] Pavlov I. *et al.* 2013. *CLEO EUROPE/IQEC*, 1.